An Iterative Two-Step Method using Thresholding and SVM to Segment Bones from Knee Magnetic Resonance Images

Alireza Norouzi[1], Narges Habibi[2], Zahra Nourbakhsh[2], Mohd Shafry Mohd Rahim[3]
1-Department of Computer Engineering, Khomeinishahr branch, Islamic Azad University, Isfahan, Iran.
Email: norouzi.arz@gmail.com (Corresponding author)
2-Department of Computer Engineering, Isfahan Branch, Islamic Azad University, Isfahan, Iran.
3-Department of Software Engineering, Universiti Teknologi Malaysia, Malaysia.

Received: 16 March 2023 Revised: 23 May 2023 Accepted: 5 June 2023

ABSTRACT:
Automatic and accurate bone segmentation has important medical applications. Thresholding-based segmentation is the most widely used method to segment the object of interest from the background. Although bone tissue is among the brightest tissues in MRI T2 images, bone has a similar intensity and comparable characteristics to particular other tissues, such as fat, which may cause misclassifications and undesirable results. We have proposed an automatic, accurate, and rapid, with less computational complexity and time segmentation method for the knee bone using iterative thresholding and Support Vector Machines (SVMs). The initial threshold value is first obtained by Otsu Thresholding to partition the image into two classes: bone and non-bone candidate areas. The SVM detected the bone region from the bone candidate areas based on location and shape. The iterative process significantly improved the thresholding value until the bone was identified. The post-processing step utilized a Canny edge filter and image opening to eliminate the undesired area and to more accurately extract the bone. The proposed segmentation technique distinguished between bone and similar structures, such as fat. The object (bone) detection rate was 1, and the average segmentation accuracy was 0.96 using the Dice Similarity Index.

KEYWORDS: Segmentation, Otsu Thresholding, SVM, MRI, Bone.

1. INTRODUCTION

Accurate and automatic image segmentation is a fundamental and challenging problem in the fields of computer vision and medical research. Better segmentation results improve the understanding of the status and progress of a disease. They provide a volumetric quantification of an organ (bone) that can potentially be utilized for the diagnosis and treatment of joint diseases. Osteoarthritis (OA) is the most common form of arthritis. OA of the knee involves the progressive degeneration of the bone and the soft tissues as well as the narrowing of the joint space, sclerosis, and the formation of osteophytes [1]. Based on statistical research, approximately 40 percent of persons above age 55 have common knee pain [1, 2]. Magnetic Resonance Imaging (MRI) is a flexible and non-invasive imaging method that is likely the optimal modality for assessing OA [3].

Certain aspects of MRI make segmentation challenging. For example, noise, connected neighboring tissue, and low contrast between certain tissues make it difficult to accurately segment the tissue with clear edges [4, 5]. In the knee, the tissues around the bone include cartilage, tendons, the meniscus, ligaments, and muscles, and segmenting particular tissues in various slices is difficult by MRI. Intensity inhomogeneity is another problem. Similar intensities and textures of various tissues lead to misclassifications in segmentation [3].

Fig. 1 depicts a typical MR slice, selected from an MRI database, that illustrates the similarities in intensity and characteristics between fat and bone. Moreover, fat has the same texture as bone. These similarities create a challenge for the segmentation task and lead to misclassifications. Another problem is that tissues have different sizes and shapes in various slices, and tissues such as bone exhibit different shapes in different individuals, making segmentation difficult. However, there is too much data to segment manually, and this has been one of the biggest hurdles for MRI analyses [6]. Generally, manual segmentation is too time-consuming for the experts [7]. Therefore, an accurate automatic segmentation method would be considerably valuable.

Paper type: Research paper
DOI: 10.30486/mjee.2023.1973270.1011
How to cite this paper: A. R. Norouzi, N. Habibi, Z. Nourbakhsh, and M. Shafry Mohd Rahim, **"An Iterative Two-Step Method using Thresholding and SVM to Segment Bones from Knee Magnetic Resonance Images"**, *Majlesi Journal of Electrical Engineering*, Vol. 17, No. 3, pp. 83-95, 2023

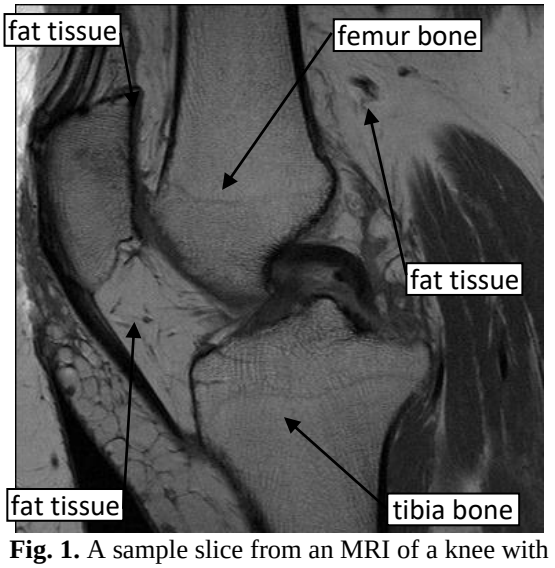

Fig. 1. A sample slice from an MRI of a knee with the bone and fat indicated.

Recently, several semi-automatic or fully automatic segmentation methods have been developed to address each of these difficulties in medical imaging. Semi-automatic methods perform the desired segmentation by obtaining the initial values and the seed points from the user, whereas fully automatic methods obtain the required initial values from the appropriate algorithms, thereby eliminating input from the user.

Various thresholding and intensity-based segmentation methods have been utilized for medical purposes on numerous body parts, such as the brain cortex, bone, cartilage, and lung. In these methods, the classification of each pixel depends on the intensity and gray level [8],[9],[10].

A semi-automatic thresholding method to segment the meniscus has been described by Swanson et al. Seed points were manually obtained within the meniscus area, and a threshold value was calculated using a Gaussian fit model [11]. Visually selecting the seed point and the threshold value can produce inappropriate results. To reduce user-dependent errors, Rathnayaka et al. proposed a novel approach for selecting an appropriate threshold value based on the Canny filter [12]. Buie et al. presented a dual-threshold method to extract the periosteal and endosteal surfaces of the cortex [13]. An iterative Otsu Thresholding scheme and morphological operation were proposed to identify a rough border of the pectoral muscle in mammograms [14].

Researchers have utilized adaptive thresholding to segment an object of interest. An adaptive thresholding method is used to segment denser masses from surrounding tissue in mammograms [15]. A local adaptive threshold method has been proposed to segment CT (Compute Tomography) images of trabecular bone [16]. Adaptive thresholding segmentation is utilized in digital angiography. Each original image is divided into two sub-images, and thresholding is applied to each one. Subsequently, the sub-images are combined to obtain the final result [17].

Since bone and fat have a greater intensity than other tissues in CT images, they can usually be separated using thresholding-based methods. Zhang et al. utilized a 3D adaptive thresholding method to segment bone in CT images. In the first step, the bone and non-bone parts of the image were divided, and the iterative process updated the voxel classification. This iterative process improved the thresholding performance [18].

The Support Vector Machine (SVM) is a type of learning machine that is utilized to segment many medical images. To segment the brain, a simple SVM classifier for feature extraction was applied to the results of an active contour model to identify brain structures in MRI [19]. SVM has been utilized to segment the knee bone using features extracted from the phase information of the MR signal [20]. In other work, SVM has been utilized to detect masses in mammograms. The enhancement and neural network prepare regions that might contain masses, and SVM classified the candidate regions into mass and non-mass classes [21]. Also, SVM has been used in knee bone classification in various articles, for example, Zhang et al. used a new classification model using a combination of extreme learning machine (ELM)-based and discriminative random field (DRF)-based in which DFR introduces spatial dependence between spatial voxels to ELM, creates and uses it to segment multi-contrast MR images of the knee bone. The results show higher accuracy in both meniscus and cartilage segmentation than in SVM, DFR, and ELM methods [22]. In another research, Thengade and Mutha combined the methods of SVM and rough fuzzy c means classifier to classify the knee cartilage for the diagnosis of Osteoarthritis, which requires the diagnosis and identification of the destruction of the cartilage of the femur and tibia, and with the gradual loss of the knee joint to occurs and causes pain and swelling of the joints and the gradual failure of the knee and inability to move[23]. Kumar and Jayanthy have used the segmentation-based technique as well as image processing techniques such as thresholding, contrast enhancement, edge detection, and histogram equalization on 2D MR images. In this method, two-dimensional images are taken, the background noise is reduced by using rough mask, feature extraction is performed using GLCM method, and texture features are calculated from the image, then these calculations are given to SVM and with this method, they were able

to perform the division with an accuracy of 86.66 [24]. Hegadi et al used the combination of SVM and KNN methods to classify and divide MR images into two classes, healthy or with OA, and was able to achieve high accuracy results compared to other methods [25]. Öztürk and Albayrak have used different techniques such as proximity-correlated (VC) sparse, uniform, VC dense subsampling, and Gaussian using 23 experimental MR images and 10 training images to generate four training models of knee bone segmentation. The results show high DSC values for VC sparse subsampling technique compared to other methods and this value for patellar cartilage is equal to 72.6%, for femoral is equal to 82.6%, and for tibial is equal to 83.1% [26].

Other methods of knee bone segmentation include machine learning and deep learning methods, which are discussed below in the articles used in these fields for knee bone segmentation. The use of artificial intelligence methods for image segmentation has problems such as class imbalance and the inability to distinguish the same anatomical structure in the segmentation between bone and soft tissues. These have been problems. For example, in 2022, in order to meet the need for segmentation, Fleflian et al. modified the R-CNN mask, which is a sample segmentation method at different scales of pathology, histology, and MRI sequences around the edges of the sample from 500 scans. In a study by Knee MRI and 97 hip MRI scans have been used in adults with symptomatic hip OA. He has improved the R-CNN mask from an additional ROIAligned decoder block in the segmentation header and connected them using a jump connection. To evaluate his method, he also used the Dice score and Hausdorf distance and was able to achieve a Dice score of 98% for the femur, 97% for the tibia, 80% for the femoral cartilage, and 82% for the tibial cartilage, which is compared to the original method. R-CNN has better results and can monitor changes in OA images, and is more sensitive to sample details [27]. In another paper, Felfeliyan et al have proposed a CycleGan-based framework for unsupervised translation of sequences in five OA scans from knee MR images, which has been used for the first time on knee MR images. This method has been able to translate TSE Fat, convert MR images to DESS, implement MaskRCNN on DESS images, and segment cartilage regions. This method has been able to automatically and unsupervisedly segment images with Dice equal to 0.73 without retraining. One of the limitations of this method is that there are fewer MRI data than manual medical images, which can be solved by collecting more MR images [28]. Gatti and Maly have used a multi-stage CNN method for MRI image segmentation. This work in two steps includes image segmentation based on the images that the output probability of each voxel belongs to the class of interest and step 1 probabilistic maps connected to the raw data on 176 OAI images and 60 healthy images. The results show that the accuracy of cartilage segmentation is 0.913 for lateral tibial, 0.907 for femoral, 0.840 for patellar, and 0.876 for medial tibial, and the accuracy of detecting healthy cartilage is 0.930 for lateral tibial, 0.938 for femoral, 0.955 for patellar and 0.911 for medial tibial which indicates very high accuracy [29]. Since CNN networks have poor segmentation results due to image mismatch such as textural and structural contrast and heterogeneity, Khan et al developed an automatic knee bone segmentation method on OA images and a method based on deep learning and CNN that consists of an encoder, they used it and were able to improve the automatic segmentation of CNNs by making changes in the knee texture and also using trimap to blur the images [30]. Also, in another article, they have presented a new deep collaborative method based on encoder-decoder-based segmentation network and its combination with a low rank tensor-reconstructed segmentation network, and also to define and model border areas with high confidence. A multipath CNN is used. Therefore, by using the secondary path with the low-rank reconstructed input, they were able to accurately identify and segment the border regions and get the results of 0.9825 overall segmentation dice score for 6 musculoskeletal tissues and 0.9 average dice exceeding for the Femoral section, and Tibial [31]. Burton et al have used semi-supervised learning, 2D and 3D CNNs, and an inference strategy called Monte Carlo patch sampling to segment six knee structures. This method has achieved 0.989 dice similarity coefficient (DSC), the average error between the predicted geometries and the ground truth is 0.56 to 0.98, and 0.978 of IoU has been achieved. It was also shown that CNNs trained by the semi-supervised method were able to perform better than CNNs trained by the supervised methods [32]. Dal et al have also used a compact CNN with shallow memory called CAN 3D to effectively reduce the number of parameters required by the model and also to perform better and more complex models. This network has the ability to maintain the integrity of data with large processing and direct 3D input and greatly reduces the calculation time. It also uses a loss function to improve accuracy in classes of unbalanced 3D images. This method has been compared with advanced UNet 3D, VNet and Enhanced UNet methods and it has been shown that this method has fewer parameters and faster results in less time and also achieved dice coefficient accuracy equal to 0.00±0.98 and 0.04±0.88 for the femur [33]. Using deep learning methods to segment the knee bone has challenges such as the need for annotation data to train the model, that is why Peng et al used a KCB-Net method to segment 3D MR images

of knee cartilage and bone which uses a small subset of cut images for annotation and creates a bridge between sparse and complete annotation. This method first selects an effective subset of slices and trains this set, then in the next step it trains another labeled 3D images by bi-directional hierarchical earth mover's distance (bi-HEMD) algorithm . The final results are adjusted by IPM and tested on four data sets OAI, iMorphics, SKI10, and ZIB and show that the proposed method can achieve 10% better results than other methods [34]. Ahn et al proposed a new segmentation algorithm with surface-based segmentation method and a new data pattern from 20 healthy individuals in OAI database and spatial fuzzy C-mean clustering. The proposed algorithm was able to achieve the results of 84.8% of dice similarity coefficients for patellar, 81.7% for tibial cartilage and 87.1% for femoral, as well as DSC results of 4.3, 3.5 and 8.8, respectively, and this algorithm has the ability to apply on three cartilage structures and can increase performance by 5% compared to other methods [35]. Some articles have also used different UNet methods. In UNet, a two-dimensional image is given as an input and a two-dimensional image is also given as an output. For example, Kasler et al. have proposed 2D and 3D UNet for automatic segmentation of cartilage bone, femur and tibia, and segmentation of bone and cartilage in one structure. They performed training on T2 images from double echo steady state (DESS) data from the publicly available Osteoarthritis Initiative (OAI) dataset with femoral and tibial bone and cartilage segmentations. In order to evaluate the proposed model, they used the criteria of boundary distance-based metric Average Symmetric Surfaces Distance (ASSD), Sørensen-Dice Similarity Coefficient (DSC) and Volumetric Overlap Error (VOE) and were able to segment in 2D UNet in 3.2 seconds and the time of 4.6 seconds for segmentation in 3D UNet also achieved 0.98 of DSC, 0.314 of ASSD, 5.662 of VOE in 2D UNet and 0.982 of DSC and 0.282 of ASSD and 5.044 of VOE in Tibial [36]. Sengara et al used four different architectures inspired by UNet and with the use of multilevel UNet to segment the knee bone from 3D knee MRI images. Also, 3 different datasets CCBR, LIRA and OAI have been used to improve the performance and evaluate the model. The research results show better Dice Score, less training and calculation time, less parameters and complexity, more accuracy and less memory in MPUNet2+ than MPUNet and other methods, and it also has less FN and PN than MPUNet [37].

More and Singla have presented an architecture based on discrete wavelet transform (DWT) and MultiResUNet called Discrete-MultiResUNet which is used for feature extraction as well as data segmentation. In this method, OA images are used, and the advantages of this method include considering more prominent features of the magnetic resonance image of the knee, and thus obtaining more details for segmentation, using the Adam optimizer, and achieving efficiency. He pointed out the direction of model training above. This method was able to achieve 96.77% of classification accuracy and 98% of dice coefficient [38]. Almajalid et al have used the modified UNet to identify the 3D MRI bone structure of the knee. This method takes several adjacent slices of the image as input, and the output is a single binary image. 99 knee MRI cases, each of which has 160 two-dimensional slices, have been used, and 97.22% Dice coefficient (DICE) has been used in the test data, as well as better performance in larger data and the best segmentation performance in 5 slices. Two left neighbors, two right neighbors and, a center slice of 352x352 pixels are obtained [39]. Kemnits et al focused on the UNet method on 250 manually trained thigh images as well as a test set of 24 bilateral thigh images from subjects with knee pain to detect OAI. The segmentation results of this method for people with one-sided knee pain less than 1 second and the dice similarity coefficient is equal to 0.01±0.96 and also $p<0.001$ and effect size: 0.69 for knee pain and $p<0.001$ and effect size: 0.73. It is for people who do not have knee pain. Therefore, the results show a speed of less than 1 second for knee segmentation in big data, while other methods have a time of 3 to 6 minutes, and even manual segmentation techniques require 60 to 90 minutes, so it can be divided to have a more precise classification than other methods [40]. Do et al also used the Seg-UNet method to segment the knee bone tumor and were able to achieve 75.42 IoU pixel results for 416x416 pixel images, 69.79% for 352x352 images, and 69.69% for 224x224 pixel images. While the SegNet method reached a result of 57.10% for 224x224 images and the Unet method reached a result of 38.26% for 224x224 images and this result shows the better performance of the proposed method compared to other methods [41].

The goal of medical image segmentation is to create a fully automated segmentation system. The main novelty of this paper is focused on two parts: the first one is presenting a linear formula based on Otsu thresholding to have a better thresholding value in order to separate bright tissues from others, which leads to better segmentation results; and the second one is proposing shape features to identify bone regions from others. The method proposed here addresses the problem of similarity between bone and fat in knee bone segmentation. Bone was detected in two iterative steps: in the first step, the thresholding technique was utilized to separate the fat and bone regions from the other background tissues based on a calculated threshold value; and in the second step, the tibia and femur were detected using multi-class SVM based on

shape and location. If an object was not confirmed in the second step, the iterative process was continued by updating the threshold value and repeating the detection step. The undesired areas were removed to obtain precise results. The proposed method has sufficient flexibility to function with different medical imaging modalities, such as CT and ultrasound, and various body parts, such as cartilage, tendon, and muscle. According to the reviews conducted on other articles, SVM has less computational complexity and has the ability to divide images in less time. On the other hand, separating femur and tibia bone which is our goal from other bright tissues is a kind of binary classification, therefore SVM which is a robust and most used binary classification method is used. The remainder of this paper is organized as follows: Section 2 provides a background review, Section 3 presents our proposed method with implementation details, Section 4 includes the experimental details and results, and the conclusions and future work are provided in Section 5.

2. BACKGROUND REVIEW

2.1. Support Vector Machine

Support vector machines are one of the most successful models of machine learning and are based on the statistical learning theory that was proposed by Vapnik in 1995 [42], [43]. An SVM is a binary classifier that classifies data based on a hyperplane. It searches for a hyperplane that maximizes the margin between two classes (Fig. 2). Training data are not always linear data. In the case of nonlinear data, the SVM classifier maps the nonlinear data into a higher dimensional space. A kernel function maps the data. Different types of kernel functions have been described, but the most common ones are the polynomial and Gaussian Radial Basis functions [44]. SVMs can also be utilized for multi-classifications in two cases [45]: one-against-one and one-against-all. If we have K groups of data in the training set, we have to apply K SVMs in the one-against-all case, and the SVMs separate one class from the other (K-1 other groups) in each run. In one-against-one, for K groups of data, K(K-1)/2 SVM classifiers are required, and each classifier separates one class from another.

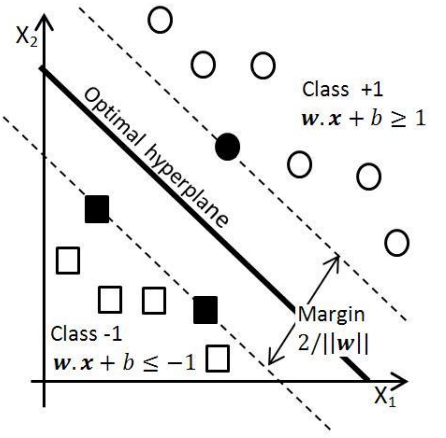

Fig. 2. SVM: linearly separated data using a hyperplane classifier.

2.2. Thresholding

Thresholding is one of the simplest and fastest segmentation methods and assumes that images comprise regions with different gray levels. The histogram of the images contains peaks and valleys that divide images into various parts. The threshold is the value in a histogram that divides the intensities into two parts, the "background" which includes pixels with intensities that are less than the threshold value, and the "foreground" which contains pixels with intensities that are greater than or equal to the threshold value. There are different methods for calculating threshold values for thresholding segmentation, such as the Otsu method. The Otsu Thresholding method calculates an optimal threshold value that minimizes the intra-class variance (the variance within the class), which is defined as the weighted sum of the variances of the two classes [46].

3. METHODOLOGY

In this study, a segmentation method for knee bone MRI is proposed. This method includes a two-step iterative algorithm that utilizes Otsu Thresholding for the initial segmentation and SVM to detect bone in the extracted areas. Then, a Canny filter and morphological operations are used to remove the undesired and misclassified regions. An overview of the segmentation framework is presented in Fig. 3.

3.1. Segmentation

In the first step, thresholding separated the bright regions from the background because bone is one of the brightest tissues in an MRI T2 image. Otsu Thresholding was utilized to decrease the dependence on the user and to obtain the automatic optimized value that classifies the image pixels into bone and non-bone regions [16].

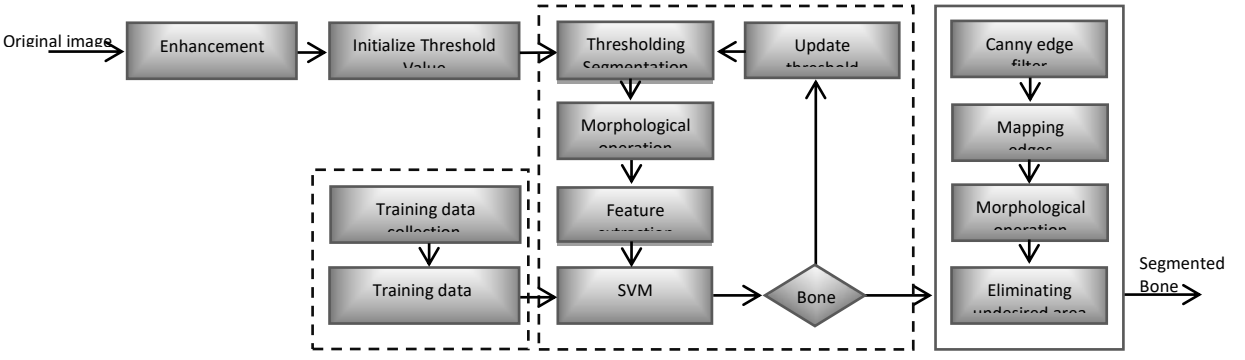

Fig. 3. An overview of the segmentation framework.

Bone candidate regions included pixels with a grey level greater than the threshold, making them more likely to contain bone, whereas the non-bone areas contained pixels with a grey value lower than the threshold, rendering them less likely to include bone. If I represents the image and x represents the image pixels, then Otsu Thresholding is applied:

$$x \in \begin{cases} B & if \quad I(x) \geq T_{Otsu} \\ \overline{B} & otherwise \end{cases} \tag{10}$$

$$I = B \cup \overline{B} \tag{11}.$$

The output of this step is a black-and-white image wherein the white regions represent bone candidate area and the black regions represent non-bone (Figure 4.b). The bone areas included bone as well as other tissues, such as fat, that have pixels of similar intensity to bone. The results obtained in the first step contained extra pixels and areas.

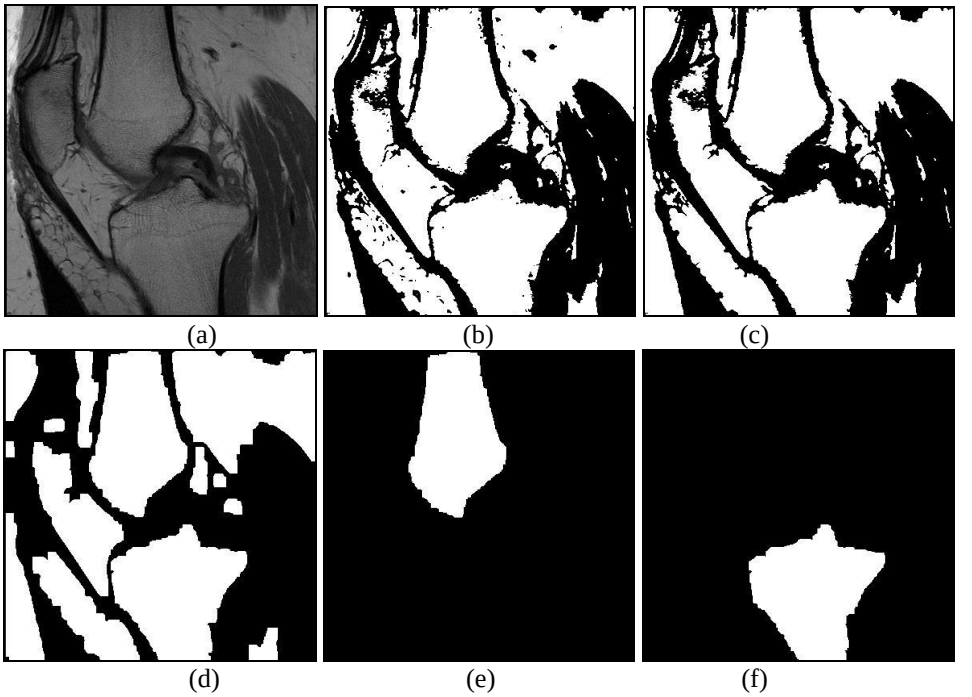

Fig. 4. An example of bone segmentation and bone ROI detection. (a) Original MRI sample slice. (b) Extracting bone candidate area using thresholding with a suitable calculated threshold value. (c, d) Applying the morphological operation to eliminate extra points and small regions. (e) Detection of the femur. (d) Detection of the tibia.

Via the morphological operation, the connected areas of less than 300 pixels were removed, and the primary bone candidate region was extracted using an image opening with a size 10 "disk" structuring

element (Fig. 4.c). If B_i represents the existing regions in the bone area, then

$$B = B_1 \cup B_2 \cup ...B_n \quad (12)$$

Where n is the number of regions in B.

The knee contains two bones, the femur and the tibia (Fig. 1). Therefore, the B_f and B_t regions represented the two existing bones in the image, and the other areas were removed.

In the second step, SVM was utilized to detect the bone area. After this step, if the output contained the tibia and femur, the desired result had been obtained. However, if the intended bones were not detected, then the selected threshold value was not appropriate. An inappropriate threshold value causes the bone area to contain numerous undesired areas, thereby adding superfluous areas to the bone and making the target tissue indistinguishable (Fig. 5). In this case, it was essential to improve the threshold value. This was achieved with the following formula, which was obtained based on experience and the training data. The following formula improves the threshold value in each iteration:

$$T_0 = T_{Otsu} \quad (13)$$

$$T_{i+1} = T_i + \alpha * T_i \quad (14)$$

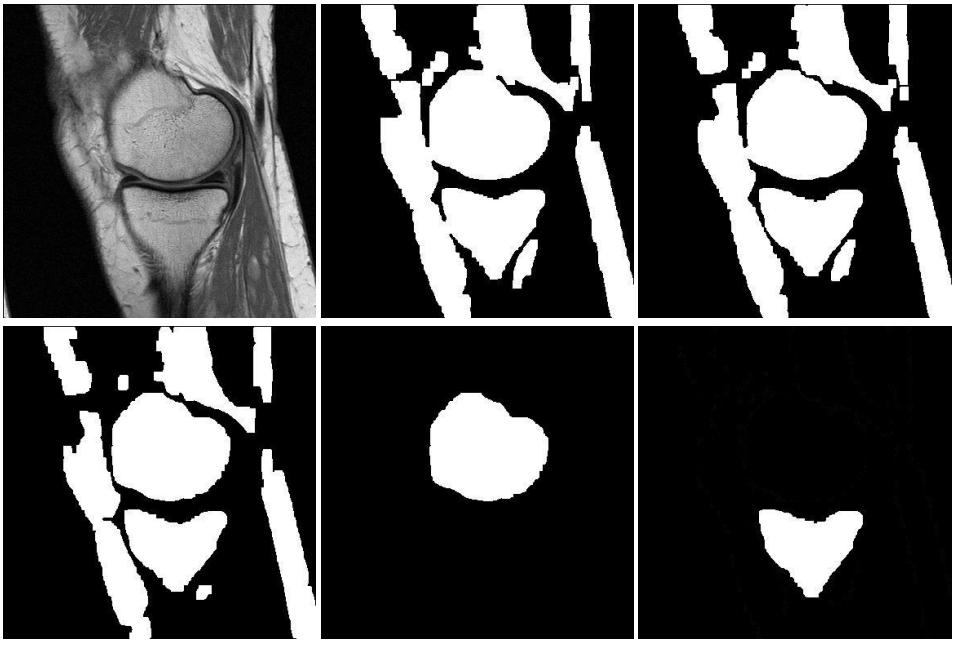

Fig. 5. Improving the threshold value in three iterations.

Where T_{Otsu} is the initial threshold value based on the Otsu Thresholding method, T_i is the threshold value in the *i*th step, and α is the scaling factor (0.05 for the femur and 0.1 for the tibia in this study).

Because similar features and characteristics among tissues lead to misclassifications, in some slices, the bone appeared with undesired and unstructured areas that were removed in a post-processing step, and the object was more precisely presented.

3.2. Feature Extraction

After a certain number of iterations, the proposed two-step algorithm provided the output, or result, for each image in black and white. Selecting the appropriate features of bone is important in the bone detection step. In this regard, the focus should be on a feature or a feature set that can efficiently extract the knee bone. Bones have a different size, shape, volume, and location in each slice. The bone is smaller in some slices compared with others, and it may be misclassified because of proximity to and similarities with fat. Therefore, features must be selected that represent bone in all the slices. In this study, 5 simple but useful features related to shape and location were selected to detect bone in all the slices. These 5 features were length, width, the distance between the topmost point of the bone and the top border of the image, the distance between the leftmost point of the bone and the left border of the image, and the number of pixels in a region (the region size) (Fig. 6).

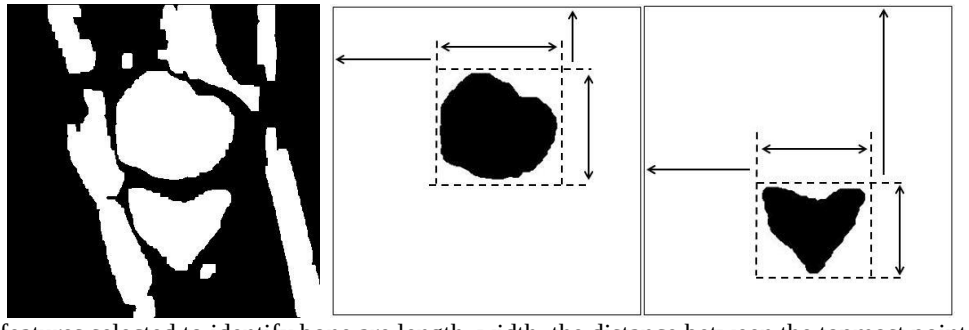

Fig. 6. Five features selected to identify bone are length, width, the distance between the topmost point of the bone and the top border of the image, the distance between the leftmost point of the bone and the left border of the image, and the number of pixels in the selected region.

3.3. Classification (bone versus non-bone)

The results obtained in the first step of the algorithm were utilized to prepare the training data. To obtain the training set, the first step of the proposed method (thresholding) was applied to all the images from a patient with an appropriate threshold value, and the results were presented as a black and white image. Subsequently, the existing areas in the image, including the tibia, femur, and other tissues, were labeled and saved along with their features in the data set. The data set was divided into two sections, the training set and the data set. Leave-N-out cross-validation was utilized to validate the SVM.

Because SVM is a binary classification method and the knee bone consists of two bones, the femur, and the tibia, it was necessary to differentiate the femur and tibia from the other tissues in two attempts using two SVM classifiers (multi-classification).

For this purpose, a Radial Basis Function (RBF) kernel was utilized with standard parameters (C=1 and y=.5) to detect the femur in the first attempt and the tibia in another attempt.

The percentage of non-bone areas which are obtained by thresholding step, is nearly 3 times more than the number of bone areas. Thus, the penalty for a bone classification error is higher than for a non-bone area.

The stepwise selection method was used to select the features and the classification was analyzed using the complete set of features.

3.4. Post-processing

After applying the proposed algorithm, the results of the bone segmentation and detection contained undesired and unstructured areas (Fig. 7). These areas existed because of the similar intensity characteristics of non-bone regions, such as fat tissue. Fig. 7.b illustrates the inclusion of a superfluous area adjacent to the femur.

To remove these areas, the Canny edge filter and morphological operation available in Matlab were utilized. First, the Canny edge filter with a threshold of 0.2 and a sigma of 4 was applied to each image to detect the related edges. Then, the edges located in regions identified as bone were mapped onto the results of the second step of the proposed algorithm. In this way, the superfluous and small regions were removed, the edges were smoothened, and the connected areas that contained two distinct tissues were split. If B_f represents the black and white image that contained bone (femur) and E is the result of applying the Canny edge filter, then

$$B_e = B_f \cap E \tag{15}$$

$$p = \{x \mid x \in B_e, B_e(x) = 1\} \tag{16}$$

Where p is the set of pixels on the edge located in the bone region. To map the edges of the bone, we considered $B_f(p) = 0$, which led to the results presented in Fig. 7.d.

In the next step, an image opening with a size 10 "disk" structuring element was employed to remove the remaining undesired areas. Finally, the bone tissue was detected by selecting the largest area in the image.

Applying this method to slices without unstructured or undesired areas can lead to the loss of useful parts of the object. Therefore, the selected slices must contain superfluous regions. Two features were used: one, the ratio of the removed area to the whole object area, and two, the number of regions created by applying the proposed method. Threshold values of 0.1 and 1 were used for these two features, respectively, to obtain the desired result. For example, if after removing the undesired area, the number of white areas in the image exceeded 1 and the ratio of the removed area to the whole image exceeded 0.1, then the final result had improved and would replace the previous result.

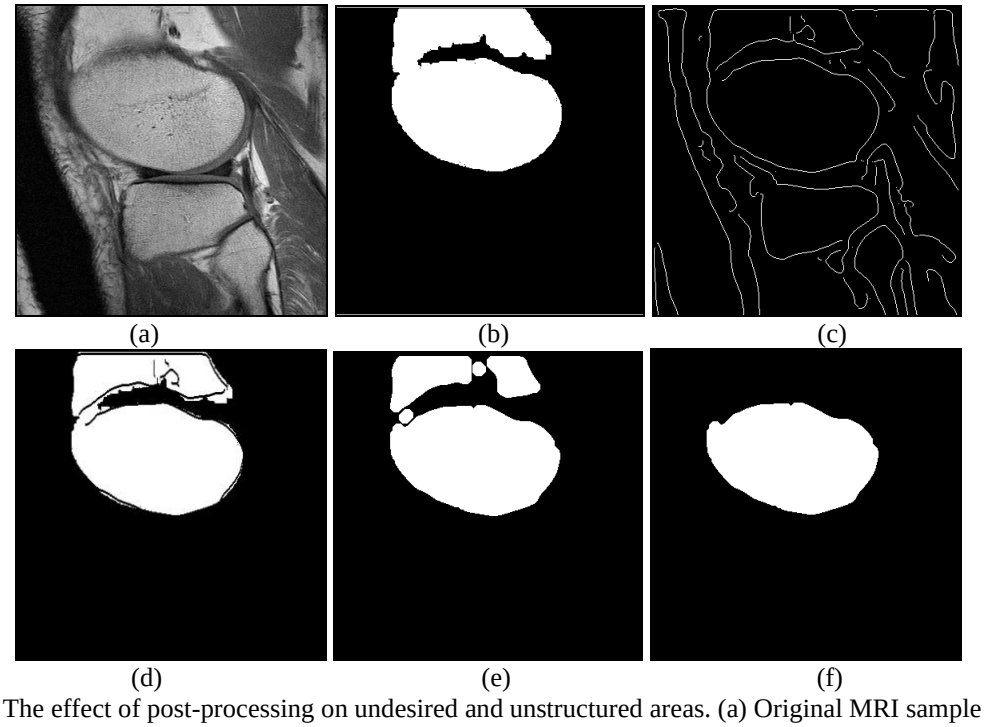

Figure 7. The effect of post-processing on undesired and unstructured areas. (a) Original MRI sample slice. (b) Detected bone, including an undesired area. (c) Edge detection. (d) Mapping the edges onto the detected bone area. (e) Applying the morphological operation. (f) Eliminating the undesired area and identifying the bone.

4. EXPERIMENT AND RESULTS

The goal of this study was to produce an automatic and accurate bone segmentation method for knee MRI images. This section presents and evaluates the results of the experiments performed according to our proposed method.

4.1. Dataset

The MR images of the knee included in this study were from the OAI dataset from the University of California, San Francisco (UCSF) [27]. The sagittal T2 images were obtained on a 3 Tesla Siemens machine. The dimensions of each slice were 384x384 pixels with pixel spacing of 0.3125/0.3125 mm and a slice thickness of 3 mm. Each set included 25-35 image slices for one leg. To obtain training data, 4 image sets were selected from different MRI sets that represented various bone sizes and appearances. Approximately 6 regions were selected as bone regions for each image slice. Thus, the training data set includes more than 600 records.

To evaluate the proposed method fifteen patients' MR images were used. For each patient, 14 slices were selected (slice number 8 to 21). In total, 210 images were tested to determine the accuracy.

To test and apply the measurement methods, a database of manually segmented images was prepared by the experts. The femur and tibia were manually segmented in each image, and the manual segmentation results were saved separately.

4.2. Validation

The accuracy of the proposed segmentation method was determined by comparing the ground truth object area of the manual segmentation performed by the experts with the automated segmentation. The Dice Similarity Index (DSI) has been used to quantitatively evaluate the performance of an algorithm [48], [49]:

$$DSI = 2.\frac{|A \cap B|}{|A| + |B|} \tag{17}$$

Where, A is the number of pixels being labeled as bone in the manual segmentation and B is the number of pixels labeled by the proposed segmentation method.

The above measurement was utilized to calculate the segmentation accuracy for each patient. More specifically, the minimum, maximum, average, median and standard deviation were used as performance measurements and to summarize the results.

In the second step of the algorithm, the SVM classification was used to detect objects from other white areas (Fig. 4.d). We defined a measurement, the object detection rate (ODR), that represents the rate of object detection:

$$ORD = \frac{S_d}{S_t} \quad (18)$$

Where, S_t is the total number of slices for each patient and S_d is the number of slices in which an object was found.

4.3. Results and Discussion

The performance of the algorithm is presented in this section. An iterative two-step algorithm was applied to a knee MRI to segment the bone. In the first step of the proposed algorithm, the bone candidate regions were identified using thresholding with an appropriate threshold value. In the second step, SVM was utilized to classify the candidate regions as bone or non-bone. Table 1 presents the ODR for each patient, illustrating the high ODR that was obtained for all the patients (100%).

Table 1. The results of 14 slices from each of 15 patients.

Patient Num.	Patient ID	ODR	Femur Avg. DSI	Tibia Avg. DSI	Both Avg. DSI	Femur Std. DSI	Tibia Std. DSI	Both Std. DSI
1	11410908	1	0.961	0.961	0.961	0.032	0.013	0.022
2	11586708	1	0.970	0.970	0.970	0.016	0.008	0.012
3	11592008	1	0.927	0.952	0.939	0.028	0.011	0.020
4	11610608	1	0.971	0.961	0.966	0.029	0.027	0.028
5	11769708	1	0.962	0.954	0.958	0.023	0.025	0.024
6	11782208	1	0.965	0.957	0.961	0.028	0.016	0.022
7	11791608	1	0.974	0.951	0.962	0.012	0.020	0.016
8	11868308	1	0.971	0.970	0.971	0.026	0.014	0.020
9	11868808	1	0.946	0.953	0.950	0.050	0.025	0.038
10	11869008	1	0.958	0.923	0.941	0.021	0.037	0.029
11	12019208	1	0.974	0.940	0.957	0.020	0.067	0.043
12	12127308	1	0.958	0.960	0.959	0.024	0.037	0.030
13	12136508	1	0.965	0.961	0.963	0.021	0.032	0.026
14	12157508	1	0.949	0.952	0.950	0.032	0.020	0.026
15	12159008	1	0.940	0.963	0.952	0.029	0.026	0.028

The segmentation accuracy was calculated using the DSI values (Table 1). The average segmentation accuracy was 0.958 for the DSI (as the most widely used measurement) and 0.96 and 0.956 for the femur and tibia, respectively. The overall median for both the femur and the tibia was 0.964. The small standard deviation (0.03) for both the femur and the tibia demonstrated the consistency of the results (Table 2). The average DSI accuracy for each slice is presented in Table 3 and illustrates the power of the algorithm for each slice.

Table 2. The results for 210 total slices (15 patients, 14 slices each).

Bone	DSI Min	DSI Max	DSI Avg.	DSI Std.	DSI Median
Femur	0.785	0.995	0.960	0.030	0.967
Tibia	0.715	0.990	0.956	0.030	0.963
Both	0.715	0.995	۰/۹۵۸	0.030	0.964

Table 3. The average DSI for each slice (power of the algorithm).

Slice Num.	Femur	Tibia	Both
8	0.976	0.965	0.971
9	0.975	0.937	0.956
10	0.967	0.948	0.957
11	0.967	0.951	0.959
12	0.962	0.958	0.960
13	0.951	0.954	0.952
14	0.962	0.953	0.958
15	0.963	0.965	0.964
16	0.952	0.960	0.956

17	0.940	0.960	0.950
18	0.945	0.956	0.951
19	0.968	0.956	0.962
20	0.968	0.955	0.961
21	0.971	0.950	0.961

Graph cut segmentation method was used by Ababneh, applied on 10 patients in the same dataset [48], [49] and achieved accuracy 95% [48], [49]. Graph cut uses cost function to obtain optimal results which needs expensive calculation. In this work, we achieved 1% more accuracy (96%) with lower running time. Moreover, the presented results show better accuracy in comparison with the deep convolutional neural network method that Liu presented for femoral and tibia bone which are 95.5% and 94.3%, respectively [50]. In a fully automated bone segmentation method presented by Ambellan, the accuracy of 86.1% to 90.4% was achieved for segmentation part for femoral cartilage which are less than the results presented in this work. [51]. In another research, the multi-stage convolutional neural networks applied by Gatti achieved accuracy of 90.7%, 87.6% to segment femur and tibia, respectively [52], that show our present method has better accuracy.

Our experiment was implemented in MATLAB on a PC with an Intel Core 2 Duo 2 GHz CPU with 2 GB of memory. The average number of iterations to segment the femur and the tibia were 1.1 and 1.2, respectively (Table 4), and the average run time of the algorithm for one image was 9.5 s (Table 5).

Table 4. The number of iterations to detect each bone.

Bone	Min	Max	Avg.
Femur	1	6	1.11
Tibia	1	4	1.20

Table 5. The run time for one slice.

Time (s)	Min	Max	Avg.	Std.	Median
One slice	3.97	19.97	9.48	2.08	8.86

5. CONCLUSION AND FUTURE WORK

We addressed the problem of knee bone segmentation from T2 MRI data. In this work, we proposed a two-step iterative method that utilizes thresholding and SVM. The initial threshold value was calculated using Otsu Thresholding segmentation and was updated in each iteration. Thresholding divided the images into non-bone and bone candidate regions. The iterative process ended when the SVM classifier identified the bone based on shape and location features. The post-processing step eliminated the undesired and unstructured areas using a Canny edge filter and a morphological operation. The real object was obtained with greater accuracy. The ODR was 1, and the overall accuracy in this study was 0.96.

Using iterative thresholding segmentation through the SVM classifier is innovative. Moreover, preparing the threshold value is different from the existing segmentation methods and adaptive thresholding methods. The proposed method is applied to sagittal T2 MRI. The method may be applicable to segment other tissues or bones. In addition, the method can present considerable accuracy in segmenting the bone from CT images. It is considerably fast and accurate to be used as a framework to identify the region of interest (ROI) for different imaging planes such as sagittal, coronal, and axial. Moreover, it is possible to prepare seed points, map shapes, and initial contours for other methods based on this framework. As a part of future work, we plan to automate the graph cut and level set segmentation using the results of this work.

6. DECLARATIONS

Competing interests: None declared
Funding: None
Ethical approval: Not required

REFERENCES

[1] Swanson, M.S., et al., "**Semi-automated segmentation to assess the lateral meniscus in normal and osteoarthritic knees***". Osteoarthritis and cartilage / OARS, Osteoarthritis Research Society*, pp. 344-53,2010.

[2] Prescott, J.W., et al. "**An Automated Method to Segment the Femur for Osteoarthritis".** in *Conf Proc IEEE Eng Med Biol Soc*. 2009.

[3] J. Fripp, S.C., S.K. Warfield, S. Ourselin, "**Automatic segmentation of the bone and extraction of the bone–cartilage interface from magnetic resonance images of the knee***". Physics in medicine and Biology*, Vol. **52**(6), pp. 1617–1631, 2007.

[4] J. Schmid, K.J., N. Magnenat-thalmann, "**Robust statistical shape models for MRI bone segmentation in presence of small field of view"**. *Medical Image Analysis*, Vol. **15**(1), pp. 155-168, 2011.

[5] A. Rudra, M.S., A. Chowdhury, A. Elnakib, A. El-baz, "**3D Graph cut with new edge weights for cerebral white matter segmentation"**. *Pattern Recognition Letters*, Vol. **32**(7), pp. 941-947m, 2011.

[6] R. Dubey, M.H., S. Gupta, "**The brain MR image segmentation techniques and use of diagnostic packages"**. *Academic radiology*, Vol. **17**(5), pp. 658-671, 2010.C. Köse, O.G., U. Şevik, "**An automatic diagnosis method for the knee meniscus tears in**

MR images". *Expert Systems with Applications*, Vol. **36**(2), pp. 1208-1216, 2009.

[7] H.D. Cheng, X.J.S., R. Min, L.M. Hu, X.P. Cai, H.N. Du, Approaches, "**Approaches for automated detection and classification of masses in mammograms".** *Pattern Recognition*, Vol. **39** (4), pp. 646 – 668.

[8] M. Ramezanpour and N. Najafabadi, "**Mass center direction-based decision method for intraprediction in HEVC standard**," *Journal of Real-Time Image Processing*, Vol. 17, No. 5, pp. 153–1168, 2020.

[9] B. Heidari and M. Ramezanpour, "**Reduction of intra-coding time for HEVC based on temporary direction map**," *Journal of Real-Time Image Processing*, Vol. 17, pp. 567-579, 2020.

[10] M.S. Swanson, J.W.P., T.M. Best, K. Powell, R.D. Jackson, F. Haq, M.N. Gurcan, "**Semi-automated segmentation to assess the lateral meniscus in normal and osteoarthritic knees"**. *Osteoarthritis and Cartilage*, Vol. **18**(3), pp. 344-53, 2010.

[11] K. Rathnayaka, T.S., M. Schuetz, B. Schmutz, "**Effects of CT image segmentation methods on the accuracy of long bone 3D reconstructions 2011"**. Medical engineering & physics, Vol. **33**(2), pp. 226-33, 2011.

[12] H.R. Buie, G.M.C., R.J. Klinck, J.A. MacNeil, S.K. Boyd, "**Automatic segmentation of cortical and trabecular compartments based on a dual threshold technique for in vivo micro-CT bone analysis"**. *Bone*, Vol. **41**(4), pp. 505-15, 2007

[13] C. Liu, C.T., J. Liu, C. Yu, S. Yu, "**A pectoral muscle segmentation algorithm for digital mammograms using Otsu thresholding and multiple regression analysis".** *Computers & Mathematics with Applications*, Vol. **64**(5), pp. 1100-1107, 2012.

[14] G. Kom, A.T., M. Kom, "**Automated detection of masses in mammograms by local adaptive thresholding"**. *Computers in Biology and Medicine*, Vol. **37**(1), pp. 37-48, 2007.

[15] ANDREW J. BURGHARDT, G.J.K., and SHARMILA MAJUMDAR, "**A local adaptive threshold strategy for high resolution peripheral quantitative computed tomography of trabecular bone"**. Annals of biomedical engineering, Vol. **35**(10), pp. 1678-1686, 2007.

[16] N. Sang, H.L., W. Peng , T. Zhang "**Knowledge-based adaptive thresholding segmentation of digital subtraction angiography images"**. *Image and Vision Computing*, Vol. **25**(8), pp. 1263-1270, 2007.

[17] J. Zhang, C.H.Y., C.K. Chui, S.H. Ong, "**Fast segmentation of bone in CT images using 3D adaptive thresholding Computers"** *in Biology and Medicine*, Vol. **40**(2), pp. 231-236, 2010.

[18] B. Tanoori, Z.A., A. Shakibafar, S. Katebi, *Brain volumetry: "***An active contour model-based segmentation followed by SVM-based classification"**. *Computers in biology and medicine*, Vol. **41**(8), pp. 619-632, 2011.

[19] P. Bourgeat, J.F., P. Stanwell, S. Ramadan, S. Ourselin, "**MR image segmentation of the knee bone using phase information"**. *Medical image analysis*, Vol. **11**(4), pp. 325–335, 2007.

[20] W.B. Sampaio, E.M.D., A. C. Silva, A.C. De Paiva, M. Gattass, "**Detection of masses in mammogram images using CNN, geostatistic functions and SVM"**. *Computers in biology and medicine*, Vol. **41**(8), pp. 653–664, 2011.

[21] Zhang, K., W. Lu, and P. Marziliano, "**The unified extreme learning machines and discriminative random fields for automatic knee cartilage and meniscus segmentation from multi-contrast MR images".** *Machine vision and applications*, Vol. **24**(7), pp. 1459-1472, 2013.

[22] Thengade, A. and B.H. Mutha. "**Image segmentation for detection of knee cartilage"**. *in 2018 Fourth International Conference on Computing Communication Control and Automation (ICCUBEA)*. 2018. IEEE.

[23] Kumar, V.A. and A. Jayanthy. "**Classification of MRI images in 2D coronal view and measurement of articular cartilage thickness for early detection of knee osteoarthritis"**. *in 2016 IEEE International Conference on Recent Trends in Electronics, Information & Communication Technology (RTEICT)*. 2016. IEEE.

[24] Hegadi, R.S., U.P. Chavan, and D.I. Navale, "**Identification of knee osteoarthritis using texture analysis, in Data Analytics and Learning".** *Springer*. pp. 121-129, 2019.

[25] Öztürk, C.N. and S. Albayrak, "**Automatic segmentation of cartilage in high-field magnetic resonance images of the knee joint with an improved voxel-classification-driven region-growing algorithm using vicinity-correlated subsampling"**. *Computers in biology and medicine*, Vol. **72**, pp. 90-107,2016.

[26] Felfeliyan, B., et al., "**Improved-Mask R-CNN: Towards an accurate generic MSK MRI instance segmentation platform (data from the Osteoarthritis Initiative)"**. *Computerized Medical Imaging and Graphics*, Vol. **97**, pp. 102056, 2022.

[27] Felfeliyan, B., et al. "**MRI knee domain translation for unsupervised segmentation by CycleGAN (data from osteoarthritis initiative (OAI))"**. in *2021 43rd Annual International Conference of the IEEE Engineering in Medicine & Biology Society (EMBC)*. 2021. IEEE.

[28] Gatti, A.A. and M.R. Maly, "**Automatic knee cartilage and bone segmentation using multi-stage convolutional neural networks: data from the osteoarthritis initiative"**. *Magnetic Resonance Materials in Physics, Biology and Medicine*, Vol. **34**(6), pp. 859-875, 2021.

[29] Khan, S., et al., "**Multipath CNN with alpha matte inference for knee tissue segmentation from MRI"**. *arXiv preprint arXiv:2109*.14249, 2021.

[30] Khan, S., et al., "**Deep collaborative network with alpha matte for precise knee tissue segmentation from MRI***". Computer Methods and Programs in Biomedicine*, Vol. **222,** pp. 106963, 2022.

[31] Burton II, W., C. Myers, and P. Rullkoetter, "**Semi-supervised learning for automatic segmentation of**

the knee from MRI with convolutional neural networks". *Computer Methods and Programs in Biomedicine*, 2020. **189,** pp. 105328, 2020.

[32] Dai, W., et al., "**CAN3D: Fast 3D medical image segmentation via compact context aggregation"**. *Medical Image Analysis*, Vol. **82,** pp. 102562, 2022.

[33] Peng, Y., et al., "**KCB-Net: A 3D knee cartilage and bone segmentation network via sparse annotation".** *Medical Image Analysis*, Vol. **82,** pp. 102574, 2022.

[34] Ahn, C., et al., "**Fully automated, level set-based segmentation for knee MRIs using an adaptive force function and template: data from the osteoarthritis initiative"**. *Biomedical engineering online*, Vol. **15**(1), pp. 1-14,2016.

[35] Kessler, D.A., et al., "**Segmentation of knee MRI data with convolutional neural networks for semi-automated three-dimensional surface-based analysis of cartilage morphology and composition".** *Osteoarthritis Imaging*, Vol. **2**(2), pp. 100010,2022.

[36] Sengara, S.S., et al., "**UNet Architectures in Multiplanar Volumetric Segmentation--Validated on Three Knee MRI Cohorts"**. *arXiv preprint arXiv*:2203.08194, 2022.

[37] More, S. and J. Singla, "**Discrete-MultiResUNet: Segmentation and feature extraction model for knee MR images"**. *Journal of Intelligent & Fuzzy Systems*, pp. 1-11, 2021.

[38] Almajalid, R., et al. "**Knee bone segmentation on three-dimensional MRI".** in *2019 18th IEEE International Conference On Machine Learning And Applications (ICMLA)*. 2019. IEEE.

[39] Kemnitz, J., et al., "**Clinical evaluation of fully automated thigh muscle and adipose tissue segmentation using a U-Net deep learning architecture in context of osteoarthritic knee pain"**. *Magnetic Resonance Materials in Physics, Biology and Medicine*, Vol. **33**(4), pp. 483-493, 2020.

[40] Do, N.-T., et al. "**Knee bone tumor segmentation from radiographs using Seg-Unet with dice loss. in Proceedings of the 25th International Workshop on Frontiers of Computer Vision (IW-FCV)***", Gangneung, Korea*. 2019.

[41] Vapnik, V., "**An overview of statistical learning theory"**. *Verlag: Springer*, 1995.

[42] Vapnik, V., "**Estimation of Dependences Based on Empirical Data"**.*Verlag: Springer*, 1982.

[43] A.R. Webb, K.D.C., "***Statistical Pattern Recognition,* ed. S. Edition"** *Malvern, UK: John Wiley & Sons*, Ltd, 2002.

[44] T. Wu, C.L., R.C. Weng, "**Probability Estimates for Multi-class Classification by Pairwise Coupling".** *Journal of Machine Learning Research*, Vol. **5**, pp. 975–1005, 2004.

[45] Otsu, N., "**A threshold selection method from gray-level histograms"**. *EEE Transactions on Systems,Man and Cybernetics*, pp. 62-66, 1995.

[46] M.C. Nevitt, D.T.F., G. Lester, "**The Osteoarthritis Initiative: Protocol for the Cohort Study"**. 2006, <http://www.oai.ucsf.edu/datarelease/>.

[47] S.Y. Ababneh , J.W.P., M.N. Gurcan, "**Automatic graph-cut based segmentation of bones from knee magnetic resonance images for osteoarthritis research"**. *Medical Image Analysis*, Vol. **15**(4), pp. 438–448, 2011.

[48] Dice, L., "**Measure of the amount of ecologic association between species"**. *Ecology*, Vol. **26,** pp. 297–302, 1945.

[49] F. Ambellan, A. Tack, M. Ehlke and S. Zachow, "**Automated segmentation of knee bone and cartilage combining statistical shape knowledge and convolutional neural networks: Data from the Osteoarthritis Initiative**", *Medical image analysis*. Vol. 52, pp. 109-118, 2019.

[50] F. Liu, H. J. Zhaoye Zhou, A. Samsonov, G. Zhao and R. Kijowski, "**Deep convolutional neural network and 3D deformable approach for tissue segmentation in musculoskeletal magnetic resonance imaging**", *Magnetic resonance in medicine*. Vol. 79(4), pp. 2379-2391, 2018.

[51] Gatti, Anthony A., and Monica R. Maly. "**Automatic knee cartilage and bone segmentation using multi-stage convolutional neural networks: data from the osteoarthritis initiative**." *Magnetic Resonance Materials in Physics, Biology and Medicine*. Vol. 34(6), pp.859-875, 2021.